P1.2 TURBULENT MIXING UNDERNEATH SURFACE WAVES

Genglin Tang* and Steven R. Long
NASA GSFC/WFF, Wallops Island, Virginia

Norden E. Huang
NASA GSFC, Greenbelt, Maryland

1. INTRODUCTION

In the interface of atmosphere and ocean, winds and ocean waves enhance the exchange of their mass, momentum, and energy. Due to the nature of viscosity of water and air, air-sea interactions cause turbulent motions in the upper ocean.

Turbulent flow is an unsteady flow with three-dimensional coherent vortical structures of various sizes (turbulent eddies) and velocities that have limited lifetimes and spatial extent. The momentum of water turbulent eddies governed by the Navier-Stokes equation can be passed on by winds across water surface. The kinetic energy of water turbulent eddies is quickly transformed into internal heat energy at Kolmogorov scales due to molecular viscosity. The energy of different scales of eddies transfers from larger to smaller until they dissipate through energy cascades.

Water turbulent velocities at any point or time cannot be predicted precisely but can be described statistically. Characteristic features of a turbulent flow include mean velocity and very intensive fluctuations.

Turbulent shear stresses have a dominant effect on the momentum balances that control the magnitude and vertical structure of air-sea interaction flows. Some researchers have experimentally and numerically investigated the effect of turbulent shear stress. Commonly used methods of experiments are either single-point or two-point velocity measurements.

* Corresponding author address: Genglin Tang, NASA GSFC/Wallops Flight Facility, Bldg. N-159/Rm. W-130, Wallops Island, VA 23337;
e-mail: genglintang@aol.com

Water surface waves are irrotational motions and cannot therefore be classified as turbulent motion. One-point measurement contaminates the wave-induced bias, which can be removed by velocity decomposition. Thais and Magnaudet (1995) reviewed these decomposition methods.

Trowbridge (1998) developed a two-point measurement method to exclude the wave-induced bias if the correlation scales of wave and turbulence are distinctively separated.

The objective of this paper was to experimentally examine the mixing layer of upper water surface induced by both wind-generated and hydraulic waves. Different scenarios were simulated in a wave tank with the capability of wind-wave-current. The wind-generated water waves are three-dimensional. Under a certain depth, the three-dimensional waves degenerate into nearly two-dimensional flow. In this paper, a two-dimensional laser Doppler velocimeter (LDV) was used to measure two instantaneous velocity components. Section 2 will introduce the apparatus and instrumentation. The test conditions will be listed in Section 3. The corresponding results will be reported and discussed in Section 4. The final section will draw simple conclusions.

2. APPARATUS AND INSTRUMENTATION

These experiments were completed in the NASA Air-Sea Interaction Research Facility (NASIRF) described by Long (1992a). In Figure 1(a), the main wind-wave-current test section is 18.29 x 0.91 x 1.22 m in length, width, and height, respectively. The test water column is 0.76 m and the remaining 0.45 m is for air flow. The maximum water current in either direction is about 51 cm/s generated by pumping up to 100 gallons/sec through the facility's 40.6 cm pipes. The water within the facility can be heated and maintained at warm temperatures. The wind was generated by a fan beyond the downwind end of the tank and returned in a closed circuit. The airflow can be cooled and humidity controlled at cool temperatures. The wind speed can go up to 18 m/s.

A wavemaker was installed across the tank at a distance 0.27 m from the upwind end of the tank, which was a rigid plate with a total height of 30.5 cm, 5 cm of which projected above the water surface and provided something of a trip to the airflow. At the bottom of the rigid plate was a flexible plastic skirt extending an additional 16 cm down. The wavemaker oscillated rectilinearly, driven by a hydraulic system using electro-servo-valves with an error-correcting feedback loop. The system was capable of following any input signal within the range of ±10V over frequencies less than 10Hz, though the rather unconventional design gave clean wave pulses only in a fairly narrow frequency range between 0.75 and 3 Hz. At the downwind end, a sloping plastic honeycomb served as a beach to absorb incident wave energy, the reflectivity over amplitudes and wavelengths used being approximately 3%.

The horizontal and vertical velocity components were measured using a conventional TSI, bench-mounted, 2-component laser Doppler velocimetry (LDV) system powered by a 5W Argon-Ion laser at the fetch of 10 m. The LDV is sited by the sidewall of the wave tank, with the capability of receiving and separating two colors of light (see Figure 1(b)). The system consists of four transmitting beams; two of them are shifted by 40 MHz using Bragg cells. The beam spacing was 130 mm. The system is operated in a backward scatter mode. A 480-mm focusing lens is used to collect the back-scattering light. The flow was then seeded with 50 μm silver contact glass spheres. Two velocity components are measured using blue (488 nm) light and green (514.5 nm) light, respectively. Two photomultiplier tubes are used to collect the scattering light of Doppler bursts, which are then fed into the two IFA 550 signal processors. A data acquisition computer is used to obtain and store data. The TSI FIND For Windows software is used to monitor and acquire the data. A calibrating wheel is used to calibrate the fringe spacing of the aligned LDV system (see Figure 1(c)).

Tests were conducted to vary the coincidence window size and sample size to study their effects on the mean velocity, the Reynolds shear stress and higher-order velocity correlations for the pure water current of 2.51 cm/s. Based on these tests, no significant differences were found in the measured variables for a coincidence window size ranging from 10 to 1000 μs, though a decreasing data rate was noted for the more stringent window sizes. A window size of 100 μs was then used. Similarly, no statistically significant differences were noted by varying the sample size from 15,000 to 30,000. Data rates of the order of 150 ~ 300 Hz were obtained while operating the system in a coincidence mode. At each measurement location, 20,000 validated samples were taken. Based on a 95% confidence interval, the uncertainty in the mean velocity (U and V) and turbulence intensities (u' and v') were estimated to be ±2.0 % or less. The uncertainty in the Reynolds shear stress was ± 7.5 %.

The wind speeds were measured at fetches of 6.75 m and 9.8 m using Datametrics differential pressure transducers attached to a three-channel Pitot tube and a two-channel hot-film anemometer that were used to measure the wind speed at heights between 8 and 18 cm above the still water level (see Figure 1(d)). The wind speed was set in these experiments at 3.8 m/s. The variation of the wind setting was ±0.2 m/s.

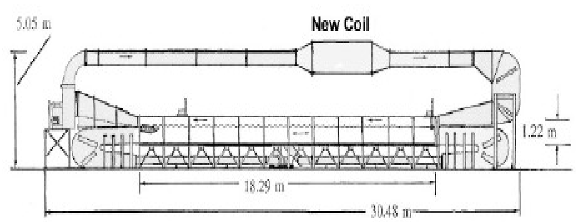

(a) Schematic of Wave Tank

(b) LDV

(c) Calibration Wheel

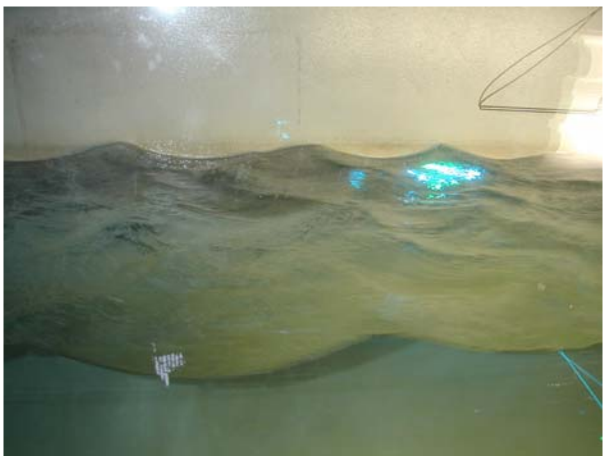

(d) Surface Wave and Hot-Film Probe

Figure 1 Setup of Wave Tank and Instruments

Measurements of wave elevations η were made using a set of capacitance wire gauges at two fetches of 8 and 8.5 m. These had a nominal sensitivity of ±0.035 mm and a good linear response (see Long 1992b). Data from the probes were digitized every 10 ms and the gauges were inter-calibrated by making simultaneous measurements in a mechanically generated 2 Hz wave train, applying a separate calibration factor to the data stream from each to equalize the value of $\overline{\eta^2}$.

The two water velocity components, wind speeds, wave elevations, hydraulic wave frequency, and hydraulic wave amplitude were recorded in another data acquisition computer.

3. TEST CONDITIONS

The wind direction is defined as positive x and vertical direction y is pointed up. The measurement station was chosen at the fetch of 10 m, where the wave and turbulent flow were fully developed. The origin was the cross point of the experimental fetch, the water surface represents y=0, and the lateral position 10 cm off the sidewall of the tank. The first point of LDV measurement was limited by the beam reflection cone at y=-7.58cm. The experiments include wind and wave but no current in the wave tank. Four cases are considered: the wind only and the wave only are baseline Case 1 and Case 2, respectively. The combinations of wind plus wave with smaller or bigger wave steepness make Case 3 and Case 4. The details are listed in Table 1. Case 3(1) and Case 3(2) were done on two consecutive days for same test condition. For the profiles of Case 1 and Case 3(1), there are 16 points with step size 1.9 cm; the experiments repeat three times at a fixed point. For the profiles of Case 2, Case 3(2), and Case 4, there were 12 points with step size 3.16 cm; the experiments repeated 5 times at a fixed point. For each test, 20,000 samples were taken.

Table 1 Test Case

Case No.	Wind velocity (m/s)	Hydraulic wave frequency (Hz)	Hydraulic wave steepness (V)
1	0	2	2
2	3.8	0	0
3	3.8	2	2
4	3.8	2	1

4. RESULTS AND DISCUSSION

Two instantaneous horizontal and vertical velocity components u and v were measured as a function of time. Because these data were obtained in the coincidence mode of the LDV, their cross product can be calculated. Mean velocity U, V, fluctuation u' and v', and mean cross-product $\overline{u'v'}$ can be calculated by Reynolds averaged methods as follows,

For Instantaneous velocity Reynolds decomposition,

$$u = U + u' \quad \text{(1a)}$$

$$v = V + v' \quad \text{(1b)}$$

mean velocity

$$U = \sum_{i=1}^{N} u_i / N \qquad \text{(2a)}$$

$$V = \sum_{i=1}^{N} v_i / N \qquad \text{(2b)}$$

where N is the number of samples; and

velocity fluctuation (root mean square of residuals in Equation (1))

$$u' = \sqrt{\sum_{i=1}^{N} (u_i - U)^2 / N} \qquad \text{(3a)}$$

$$v' = \sqrt{\sum_{i=1}^{N} (v_i - V)^2 / N} \qquad \text{(3b)}$$

The cross product (called pseudo Reynolds shear stress because the residual does not represent the true turbulence component in Equation (1)) follows as

$$-\overline{u'v'} = -\frac{1}{N} \sum_{i=1}^{N} (u_i - U)(v_i - V) \qquad \text{(4)}$$

The correlation coefficient of pseudo Reynolds shear stress is given by

$$R_{uv} = -\overline{u'v'} / |u'||v'| \qquad \text{(5)}$$

The fluctuation velocities u' and v' from Reynolds decomposition are invalid to represent the turbulence intensity under the wave conditions. For this paper, the Reynolds decomposition method is used to report and discuss the qualitative results. The effect of turbulent shear stress can be explained without ambiguity. However, it may reflect the physical trend qualitatively.

In figures 2a and 2b are shown the typical instantaneous velocity components u and v at y=-25cm for Case 3. Obviously, the fluctuation of velocity components was unlike the typical wall-bounded boundary velocity distributions because of wave-induced pseudo turbulence. The wind-generated wave and hydraulic wave had different wavelengths. The waves contaminated the flow velocity at the measurement stations. The data were also acquired unevenly so that the measured velocity could include a portion of wave velocity at various phases at a given point. Accordingly, the u and v plots reflect the unsteady structure of wave influences.

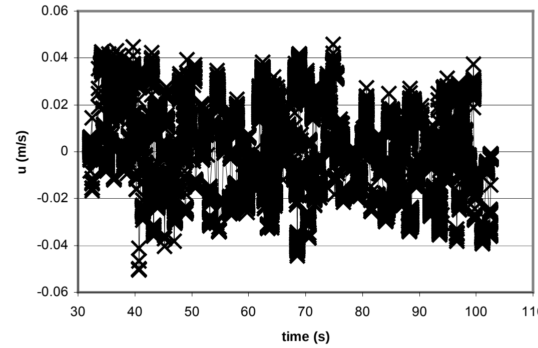

(a) u

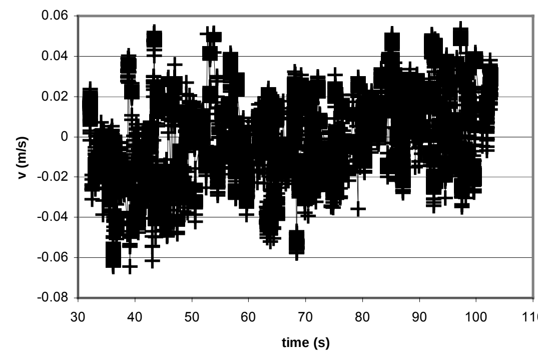

(b) v

Figure 2 Instantaneous velocities

Figure 3a and 3b represents the mean velocities U and V. For the same test condition of Case 3, two sets of data were taken at two different days (Case 3(1) and Case 3(2)). For each test at a given point, three or five sets of data were taken. The different data sets at the same station were not repeatable. The mean velocity U and V were not ergodic statistically. The mean U and V reflect the physics of different test conditions. For the wave only (Case 1), both mean U and V are fairly close to zero for the measured depth, indicating no apparent water current besides Stoke drift. It confirms that the hydraulic wave only without blowing wind is irrotational motion so that there is no turbulent flow. The characteristic of mean velocity reveals the wave nature of the flow of interest and data were taken at all phases of waves, but the total average of all samples could not converge for various phases. For the wind only (Case 2), the magnitude of V is smaller than that of U. The signs of U and V exchange around y=-28 cm. The wind generates waves and also circulatory current due to a non-slip condition of the interface between the air and water. For the superimposed cases of wind and wave, the U and V become very complicated. Two runs of Case 3 at two different days are very scattered. However, for smaller steepness (Case 4), the mean U and V drop progressively fast along the water depth. The smaller steepness means a shorter wavelength so that the penetration is shorter.

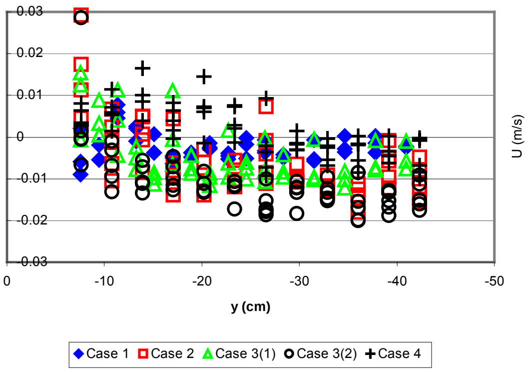

(a) U

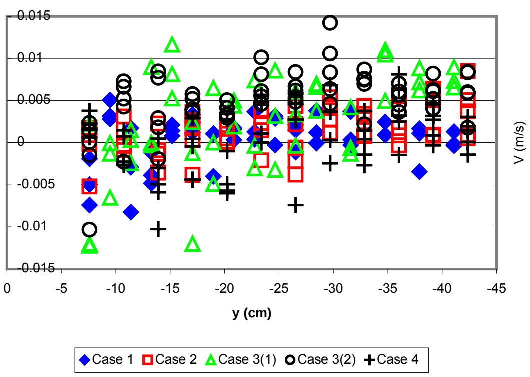

(b) V

Figure 3 Mean Velocities

Figures 4a and 4b clearly demonstrate the decay of u' and v' along the water depth. At the upper limit of the measured range, the magnitude of the wind only (Case 2) is smallest while the magnitude of the wind plus the bigger wave steepness (Case 3) is the biggest. The wave only (Case 1) is the second because its wave steepness is bigger than that of Case 4. Unlike the scatter of U and V, the u' and v' are clustered for two runs of Case 3 while the value of u' and v', closest to the surface and the penetration height of decay of u' and v', reveal the substantial effect of surface wave steepness.

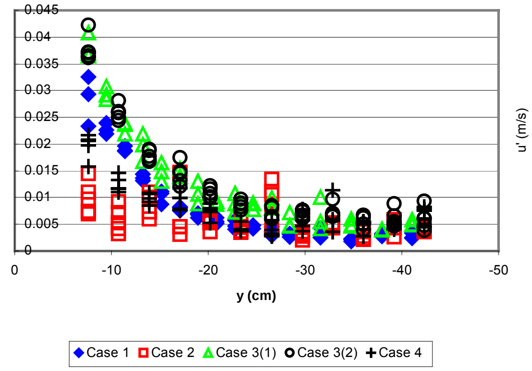

(a) u'

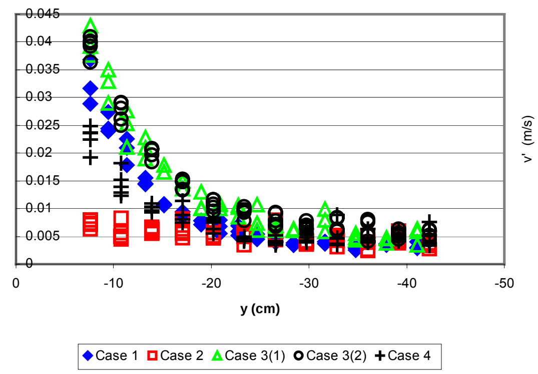

(b) v'

Figure 4 Fluctuation Velocities

Figure 5 shows the pseudo Reynolds shear stress $-\overline{u'v'}$ like the mean velocity for Case 1. $-\overline{u'v'}$ is also flat zero for whole water depth which confirms that the wave motion is not turbulent motion. For the other three cases, the patterns of $-\overline{u'v'}$ are similar; their magnitudes have peaks at the closest surface and then slowly damp out as the water depth increases.

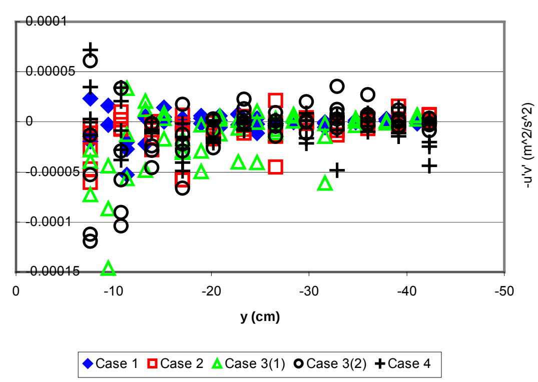

Figure 5 Pseudo Reynolds Shear Stress $-\overline{u'v'}$

The correlation coefficient R_{uv} of $-\overline{u'v'}$ is illustrated in Figure 6. Among four cases, the smallest range of R_{uv} is for the wave only (case 1) and the biggest range of R_{uv} is for wind only (case 2). With the growth of water depth, it is very interesting that the magnitudes of R_{uv} increase with the growth of water depth for Case 3 and 4 and bigger than that of the wind only case (Case 2) at the lower part of the measured profiles. This signifies that the wave influence weakens but the second circulation current is dominant in this region.

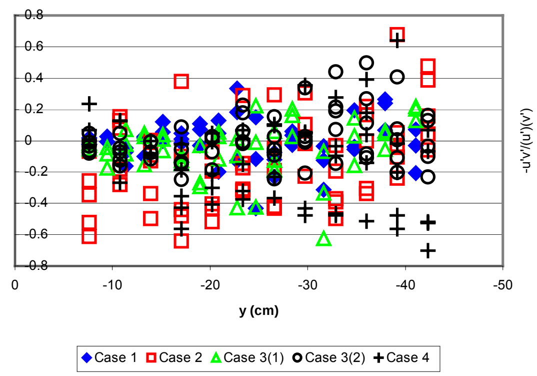

Figure 6 Correlation Coefficient R_{uv}

The quantities U, V, u', v', $-\overline{u'v'}$, and R_{uv} convey information of different roles of wind or wave. It is a fact that wind shear generates wave and turbulent current. When hydraulic waves are added to the wind-generated waves, the complex interactions occur (also see Chu et. al, 1992). Turbulent shear stress is a good indicator to describe the air-sea interactions. Thais and Magnaudet (1996) found that the combination of wind and wave has stronger turbulent shear stress in the upper water surface.

The scatter of data points reflects the wave characteristics. The complex data decomposition was necessary to extract true turbulence. The wave frequency and the wind speed are other factors to be included in future tests.

5. CONCLUSIONS

The preliminary experiments discovered some features of upper turbulent mixing layer in air-sea interaction in the laboratory. The wind only case demonstrated the typical effect of turbulent shear stress. The wave only case confirmed that the wave is not turbulent motion. When the wave was added to the wind, the air-sea interactions were enhanced and became more complicated. With the enhancement of steepness, the interactions were also enhanced. To understand the turbulent mixing under the combinations of wind and wave, velocity decompositions are necessary to remove the wave-induced fluctuations.

ACKNOWLEDGEMENT

This research was supported by the University Programs Office of NASA Goddard Space Flight Center through the National Research Council Research Associateship Programs.

REFERENCES

Long, S. R., 1992a: NASA Wallops Flight Facility: Air-Sea Interaction Research Facility, NASA Tech. Ref. Publ. RP-1277, 36 pp.

Long, S. R., 1992b: A Self-Zeroing Capacitance Probe for Water Wave Measurements, NASA Tech. Ref. Publ. RP-1278, 52 pp.

Chu, J. S., Long, S. R., and Phillips, O. M. 1992: Measurements of the interaction of wave groups with shorter wind-generated waves. J. Fluid Mech., 245, 191–210.

Thais, L. and Magnaudet, J. 1996: Turbulent structure beneath surface gravity waves sheared by the wind. J. Fluid Mech., 328, 313–344.

Thais, L. and Magnaudet, J. 1995: A triple decomposition of the fluctuating motion below laboratory wind water waves J. Geophys. Res. Vol. 100 , No. C1 , p. 741-756.

Trowbridge, J. H. 1998: On a Technique for Measurement of Turbulent Shear Stress in the Presence of Surface Waves, J. Atmos. and Ocean. Technology, 15, 290-298.